Chapter 4
MEIS Investigation of Thulium Silicide

4.1   Introduction

As described in Chapter 1, two-dimensional rare earth silicides have attracted
much attention in recent years, with numerous studies being published. The
electronic similarity of all trivalent rare earth metals leads to an expectation that
they will all form such structures, as has already been seen to be the case for a
large number. The general structure of such silicides is shown in Figure 4.1. The
number of structural studies has led to some speculation of a possible trend in
structural parameters across the rare earth series (see Chapter 5 for further
discussion of such trends). Tm lies towards one end of this series, being one of
the heavier trivalent rare earths. Although several [1-3] studies of thicker Tm
silicides have been reported there is no study of a two-dimensional Tm silicide.
A study of Tm silicide in the monolayer regime may therefore further reveal any
structural trend in the series as well as confirming another rare earth which might
be used to form such structures in technological applications. Initial
investigations [4] suggested that Tm does indeed form such a silicide but seemed
to show a discrepancy with the expected trend, which led to the careful medium
energy ion scattering study described here. The technique is ideally suited to
quantitative structural investigations of these rare earth silicides.

4.2   Experimental Details

All samples were prepared *in situ* at the Daresbury Laboratory MEIS Facility
(see Chapter 2 for details of the facility) under UHV conditions with a base
pressure of around 1×10^{-10} mbar. Si (111) samples, approximately 10×10 mm^2,
were cut from lightly doped 100 Ω cm, *n*-type wafers. The samples were cleaned
by repeated e$^-$-beam rapid heating to 1200 ˚C for approximately one minute

Original in colour

Si$_1$
Si$_2$
RE
Si$_3$

Substrate Si
Top Bilayer Si
Rare Earth

[111]
[1$\bar{2}$1]
[$\bar{1}$01]

[111]
[$\bar{1}$2$\bar{1}$]
[$\bar{1}$01]
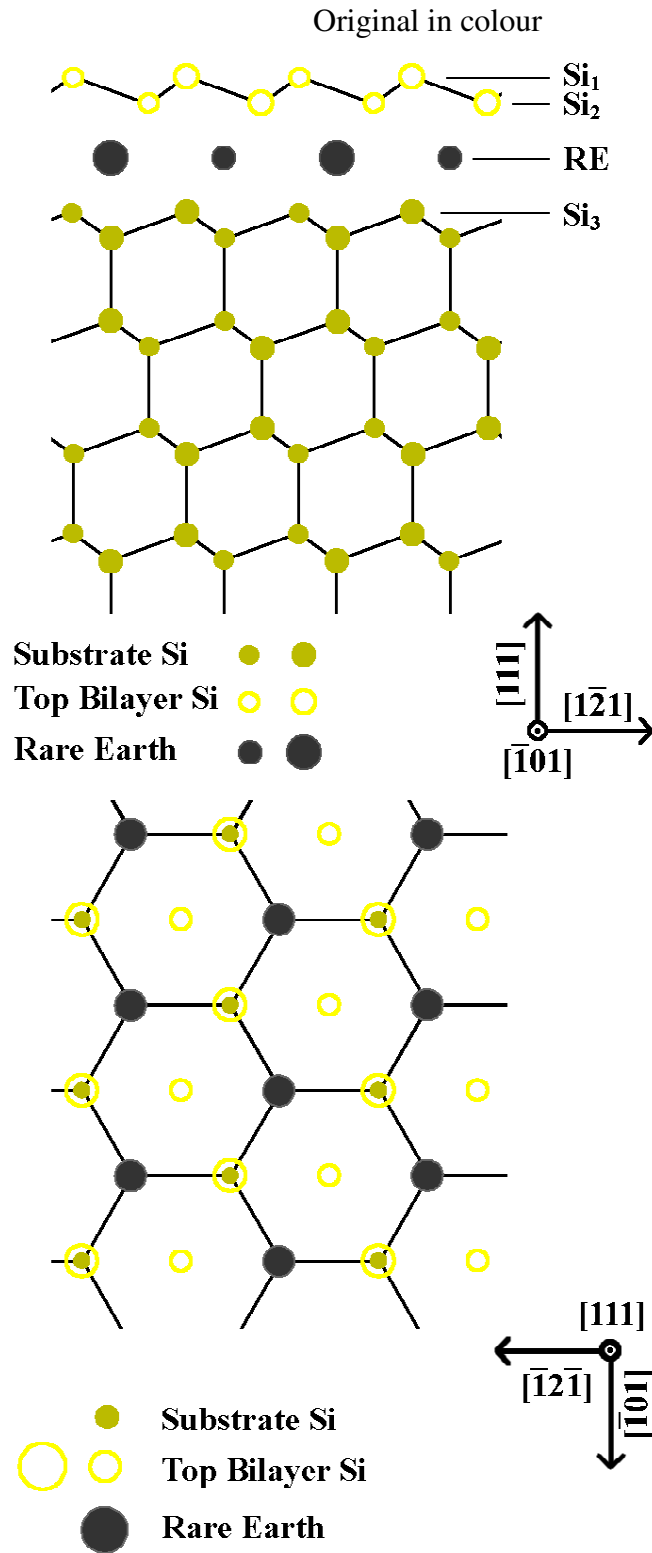
Substrate Si
Top Bilayer Si
Rare Earth

Figure 4.1: Structure of 2D rare earth silicides. The RE forms a single atomic layer located in T4 sites above the bulk Si. The silicide is terminated by a bulk-like Si bilayer (Si$_1$ and Si$_2$) which is rotated by 180° with respect to the bulk. a) side view, b) the view along the surface normal (i.e. top view).

followed by slow (<100 °C min^{-1}) cool down to room temperature. Sample temperature was monitored using an infra red pyrometer. The cleanliness of the Si (111) samples was confirmed by the presence of a sharp 7 × 7 LEED pattern. Auger electron spectroscopy also confirmed a lack of surface contamination by such impurities such as oxygen and carbon.

Tm was deposited onto the clean, newly prepared 7 × 7 surface by evaporation from a tungsten boat arrangement of an in house design. The samples were at room temperature during the deposition. The pressure during Tm evaporation was less than 1×10^{-9} mbar. The rate of Tm evaporation was approximately 6 min/ML. Again AES showed no surface contamination after Tm deposition. LEED of an as deposited sample produced only a diffuse pattern with no evidence of order. The samples were e^{-}-beam annealed to approximately 500 °C (as measured using the infra red pyrometer) for ten minutes and allowed to cool to room temperature. A sharp 1 × 1 LEED pattern was taken as indicating that an ordered surface reconstruction had successfully formed.

Samples were transferred under UHV conditions into the scattering chamber where they were placed on the precision goniometer in front of the incoming ion beam. The ion beam consisted of 100 keV H^{+} ions. The sample was aligned so that the beam was incident along a low index crystallographic direction, and scattered ions were detected around another low index direction in double alignment experiments. Two such scattering geometries were utilised, namely [$\bar{1}$ 00] incidence direction, with the detection around the [$\bar{1}$ 11] direction and the time reversed path of this (hereafter referred to as [$\bar{1}$ 00]/[$\bar{1}$ 11] and [1$\bar{1}$ $\bar{1}$]/[100]). These geometries are illustrated in Figure 4.2. The MEIS data could be used to further confirm the cleanliness of the sample, and the clear blocking dips in the angular cross section confirmed an ordered surface reconstruction. Complete data sets were collected with a beam dose of 10^{16} ions cm^{-2}, the beam size was approximately 0.5 mm × 1 mm normal to the beam. The samples were systematically moved in the z-direction (i.e. while maintaining the double
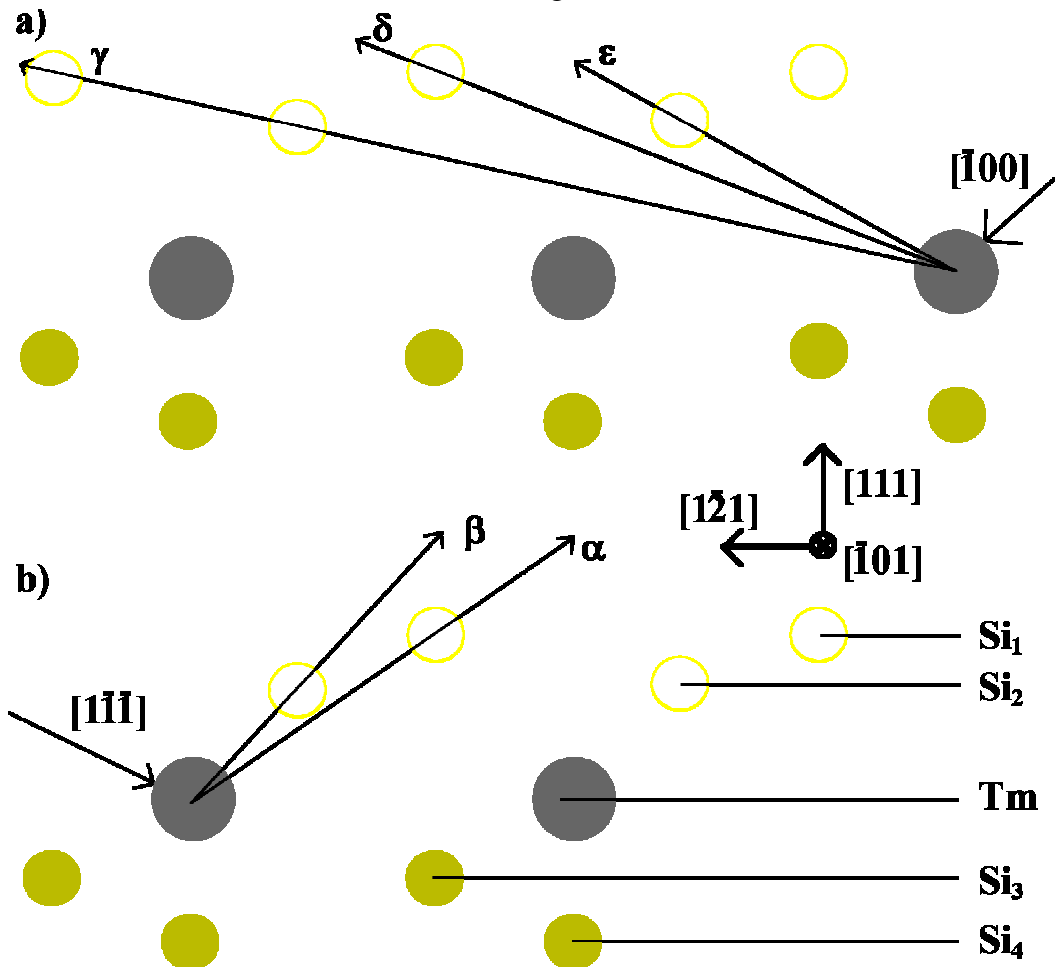
84

Original in colour

Figure 4.2: The origin of the blocking dips in the Tm signal in the two scattering geometries indicated. a) [Ī 00]/[Ī 11] b) [1Ī Ī]/[100]. The arrows indicate the origin of the blocking features labelled in Figure 4.5. Refer to Figure 4.1 for further details of the structure (note that in this figure only those atoms within the scattering plane are shown). Notice that ε depends only on Si_2.

alignment scattering orientation) between data sets in order to minimise sample damage.
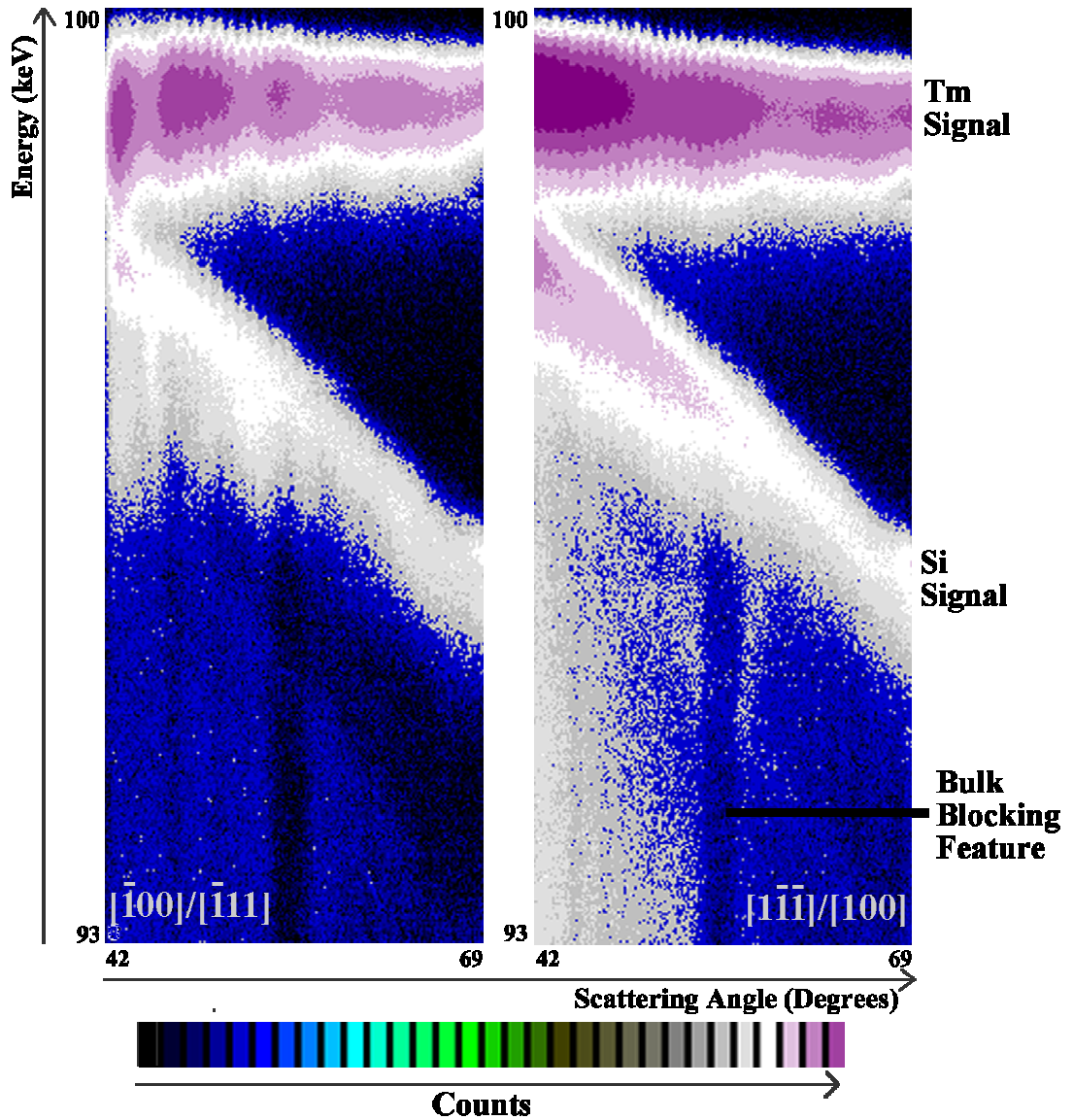
Original in colour

Figure 4.3: Typical MEIS spectra from the Tm silicide for the two experimental geometries employed (left [1̄ 00]/[1̄ 11]; right [11̄ 1̄]/[100]). The separation of the Tm and Si signals, and the bulk blocking features are all clearly visible. The Tm signal shows decreased intensity at scattering angles at which blocking has occurred.

4.3   Results and Discussion

4.3.1   Experimental Results and Analysis

Typical MEIS spectra for the two scattering geometries are shown in Figure 4.3. In both cases the signal from ions scattered from the Tm can be clearly resolved from that of those scattered from the Si, as indicated. This is due to kinematic effects as discussed in Chapter 3. Ions scattered with lower energies have been scattered from the bulk Si. The blocking feature along the detection direction in this bulk signal can be seen, and is a useful calibration tool. Even within these raw MEIS spectra, a reduction in counts at certain scattering angles can be seen within the Tm signal, indicating angles at which the scattered ions have been blocked.

The MEIS spectra were analysed by first integrating the number of scattered ions as a function of angle over an energy range corresponding to those ions scattered from bulk Si. This angular cross section thus encompassed the bulk blocking features. Comparison of these cross sections to Monte Carlo computer simulations of scattering from bulk terminated Si allowed the position of the bulk blocking features to be fitted and hence any mechanical offset in the analyser position to be corrected for. An example of such a comparison is shown in Figure 4.4. Note that here it is the fitting of the bulk blocking feature (in the direction around which ions are being detected), especially in terms of angular position, which is particularly important, as this gives the mechanical offset of the analyser. These bulk blocking features are labelled in Figure 4.4. The fact that the simulated surface is bulk terminated Si, which is obviously not the experimental case, results in some features in the simulated scattering curve (such as those around 43–46° in the $[\bar{1}\,00]/[\bar{1}\,11]$ geometry) which are not clearly evident in the experimental data. Conversely the ordered overlayer above the bulk silicon may cause weak blocking features in the experimental data or otherwise affect the scattering curve in a way not reproduced by the simulation. Such effects are responsible for the experimental features seen around 43–47° in
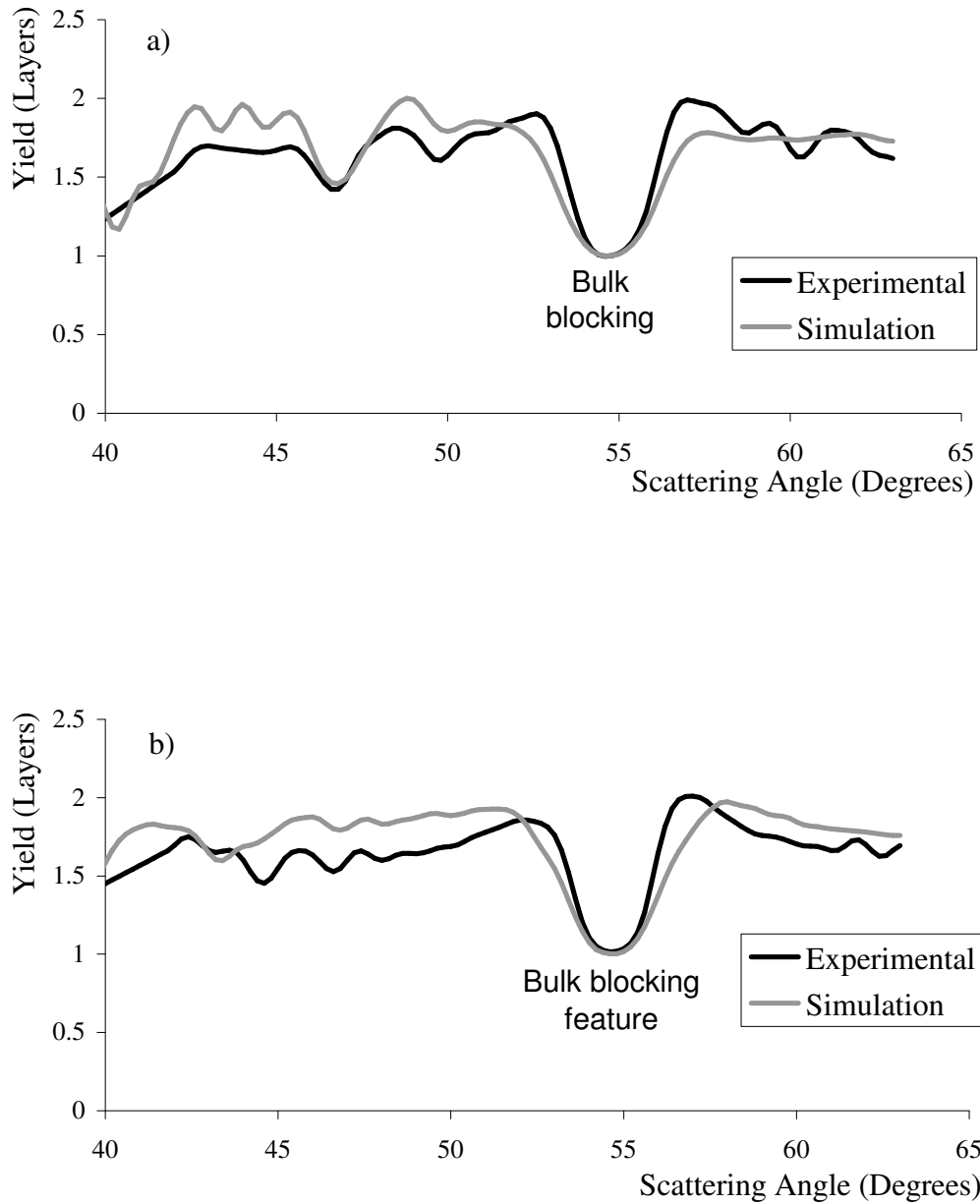
Figure 4.4: The comparison of a simulation of bulk terminated Si (111) to the experimental angular cross section through the bulk scattered ion signal, with angular offset applied. Matching the postition of the bulk blocking feature allows the angular scale to be calibrated correcting for any mechanical offset of the analyser. (a) [$\bar{1}$ 00]/[$\bar{1}$ 11] (b) [1$\bar{1}$ $\bar{1}$]/[100].

the $[1\bar{1}\,\bar{1}]/[100]$, for instance. The experimental data also exhibits further small fluctuations due to noise.

The signal from ions scattered from the Tm was also integrated as a function of scattering angle. The scattering yields from similar data sets were summed to improve the signal to noise ratio. These angular projections were then corrected for the mechanical offset determined from the above bulk fitting as well as for the kinetic energy loss factor (the so called "k^2 correction"). A final correction was applied to remove the effect of the fall off in counts due to the Rutherford scattering cross section. The corrected Tm signal cross sections for the two geometries are shown in Figure 4.5. For comparison purposes the corrected cross section from the Ho signal from a 2D Ho silicide [5] is also shown. The similarity in blocking dip position, size and shape clearly indicate that the Tm silicide has a very similar structure to the Ho silicide, as was expected due to the number of trivalent rare earth metals previously seen to form such two-dimensional silicides. Note that the main blocking features labelled α–ε and the overall shape of the curves are the most important features in terms of structural information and smaller fluctuations within the scattering curves are mainly due to noise.

4.3.2   Computer Simulations

The similarity of Ho and Tm blocking curves suggested that a 2D Tm silicide had indeed formed. In order to confirm this and to fully determine the surface structure of the Tm 2D silicide a series of Monte Carlo computer simulations were performed for each double alignment geometry, using the VEGAS code [6]. The known structure of the two dimensional Ho silicide [5] was taken as a starting structure for these simulations, the Ho being replaced by Tm. Within the simulations two parameters were allowed to vary independently; namely the vertical (z-) positions of Si_1 and Si_2 (i.e. the two atoms forming the top, reversed bilayer, see Figure 4.1). The z-positions of these two atoms were varied whilst holding the other atomic positions fixed. This is a useful approach in the MEIS study of 2D silicides: As the Tm forms a single atomic layer below the reversed
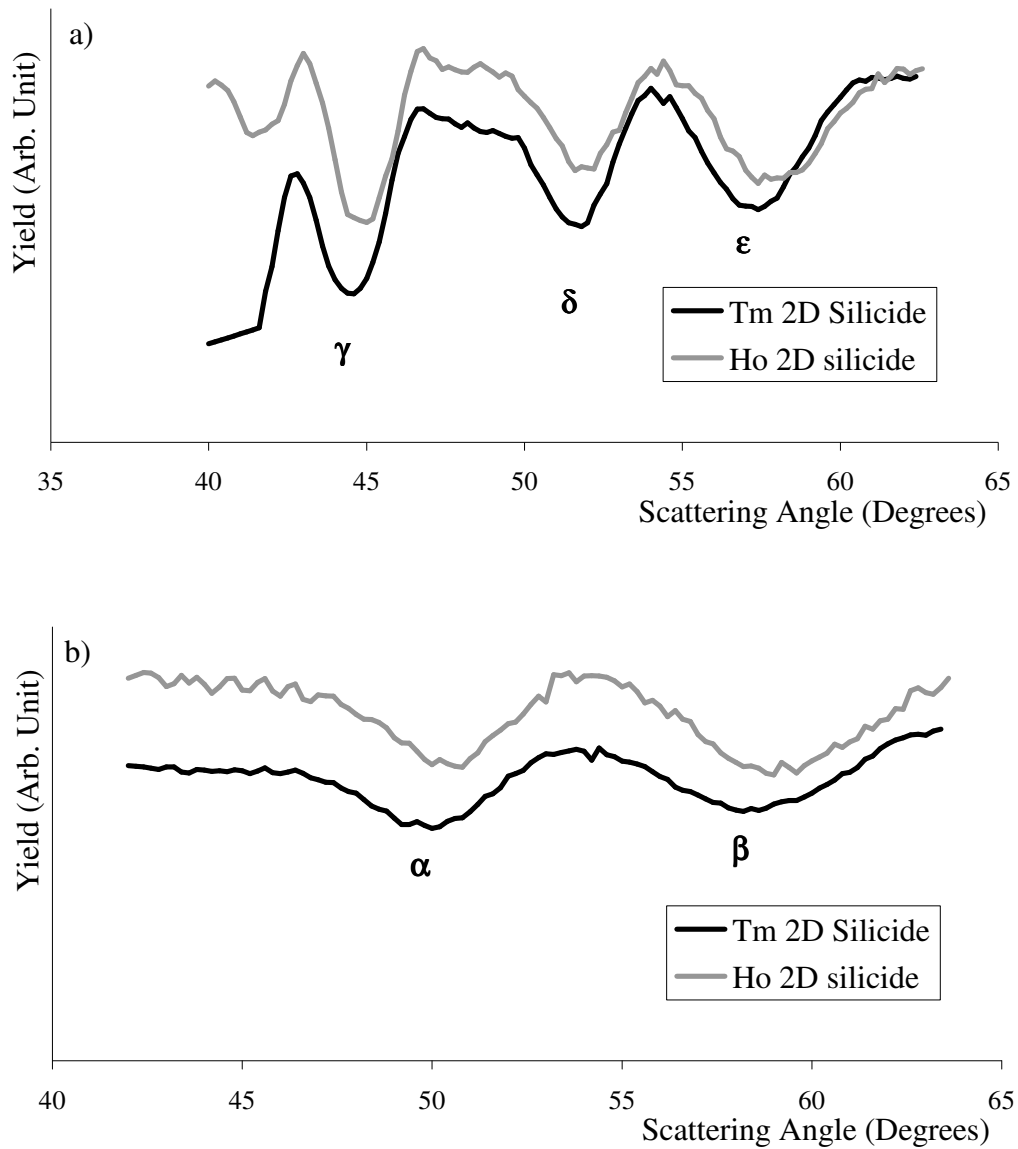
89

Figure 4.5: The corrected angular cross section through the Tm signal for the (a) [Ī 00]/[Ī 11] geometry and (b) [1Ī Ī]/[100] geometry. The curves have been corrected for the angular offset and the fall off in counts due to Rutherford scattering cross section, and scaled to an arbitrary value. Also shown for comparison purposes is the experimental cross section through the Ho signal from a 2D Ho silicide [5]. The similarity of the two curves indicates the structures are very alike, as expected. The small fluctuations within the curves are experimental noise. The labelling of blocking dips refers to Figure 4.2.

bilayer, but above the other, bulk like Si layers, it is only these two top atoms which contribute to blocking features in the Tm signal. Indeed geometrical considerations (Figure 4.2) show that some blocking dips are due to scattered ions being blocked only by Si_1 atoms or only by Si_2 atoms.

Initially the thermal vibrations of the atoms were estimated from the Debye temperatures [7] for Si and Tm (giving rms vibrational amplitudes of 0.085 Å and 0.080 Å respectively). The thermal vibrations of the top two atoms forming the reversed bilayer were enhanced by a factor of $\sqrt{2}$ over the bulk values.

Comparison between the simulations and experiment was performed by allowing the experimental counts to be freely scaled to the simulation yield. Experiment and simulation were then compared using the χ^2 R-factor

$$R_\chi = \frac{1}{N} \sum_{n=1}^{N} \frac{\left(I_{exp} - I_{sim}\right)^2}{I_{exp}} \qquad (4.1)$$

where I_{exp} and I_{sim} are the scaled experimental and simulation scattering yields, respectively. This has the advantage that its statistical basis gives a ready estimate of the error in the derived value for each structural parameter a_j, given by

$$\sigma_j^2 = 2/(\partial^2\chi/\partial^2 a_j) \qquad (4.2)$$

R-factors from all available geometries were combined to give an overall best fit. Further discussion of R-factors can be found in Chapter 5.

The first simulations consisted of a "multicalc", performing a wide search of parameter space, varying the positions of Si_1 and Si_2 as described. The atoms were moved independently in 0.02 Å steps in the z-direction (i.e. perpendicular to the surface), over a range of ± 0.20 Å from the starting position. This resulted in 441 structural models for each geometry. The experimental data for each geometry was compared to the appropriate simulations and the R-factors

calculated to produce an "R-factor curve" (a graph of the calculated R-factor versus simulation number). The R-factor curves from each geometry were then combined to produce an overall R-factor curve. The structural model with the minimum overall R-factor was then used as a starting point for further simulations. A set of simulations were performed varying the thermal vibrations of the top two Si atoms and the Tm. The best fit model produced thermal vibrations of 0.12 Å, 0.12 Å and 0.08 Å for Si_1, Si_2 and Tm respectively. Thesethermal vibrations were used in another multicalc around the so far best fit structural model. This sequence of simulations again varied the z-position of Si_1 and Si_2, over a range of ± 0.04 Å and ± 0.02 Å respectively, both in 0.01 Å steps. A final set of simulations around this best fit solution from these simulations confirmed convergence upon that structural model.

The comparison between experiment and simulation for the final best fit model is shown in Figure 4.7. The structural parameters for this model are listed in Table 4.1 and shown in Figure 4.6
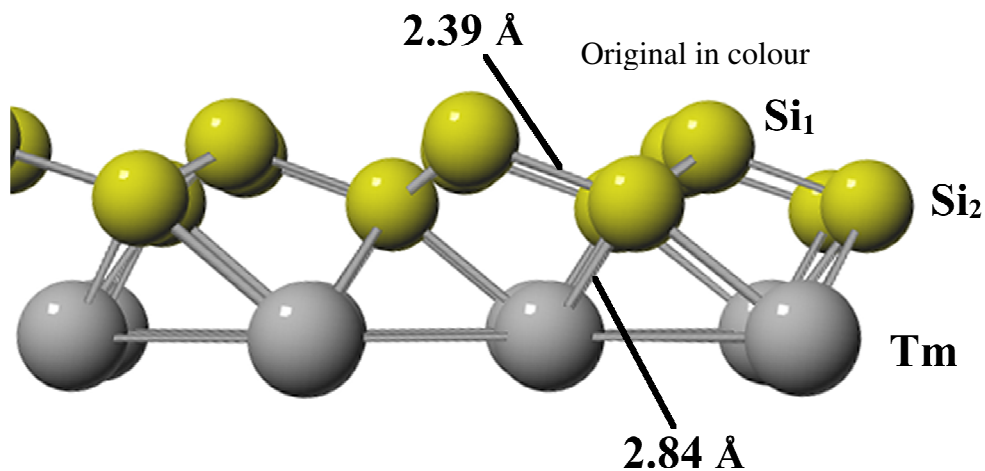

Figure 4.6: Ball and stick representation of the Tm 2D silicide surface, showing the bond lengths of Table 4.1.
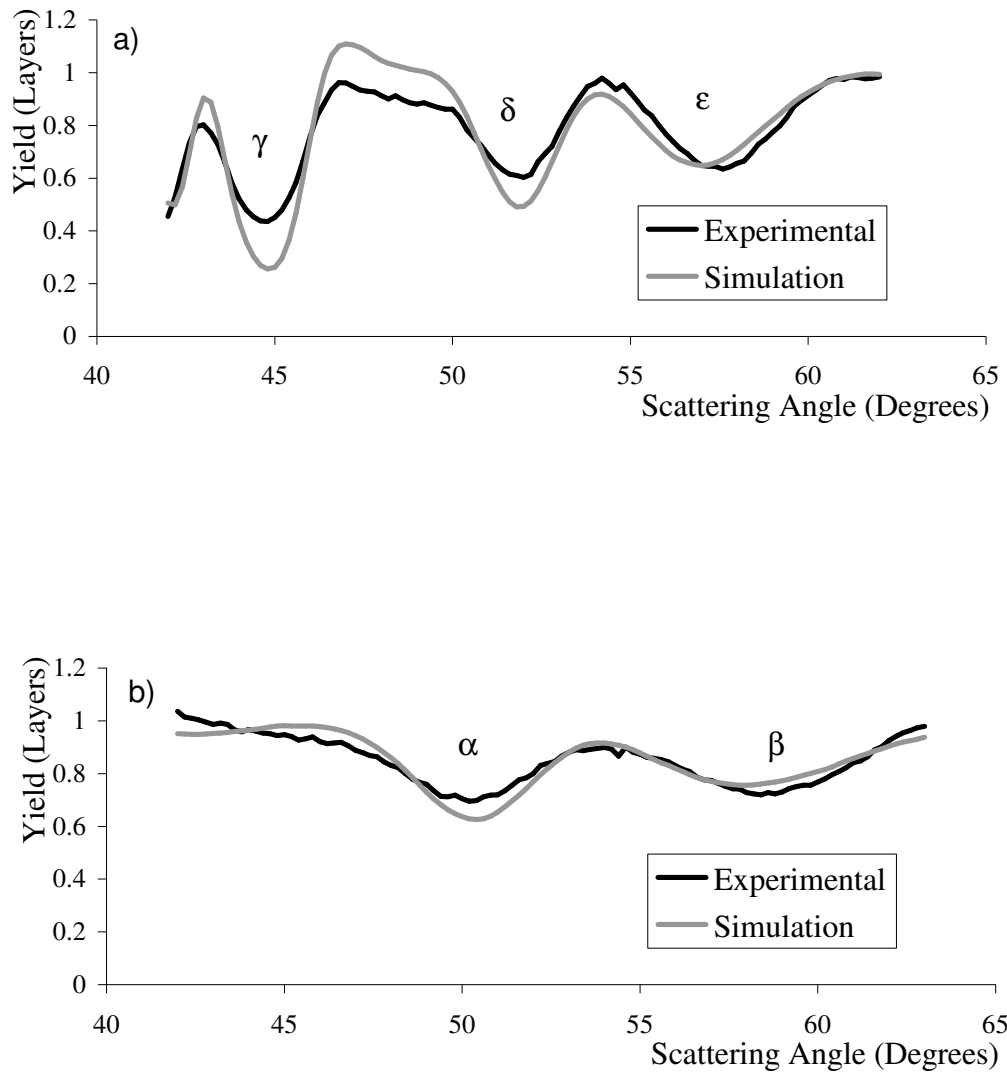
Figure 4.7: Comparison between experimental data and the simulated scattering curve for the initial structural solution for 2D Tm silicide (note that for ease of display the curves have been corrected for the fall off in counts due to the Rutherford scattering cross-section). The experimental data has been freely scaled to the simulation. (a) [$\bar{1}$ 00]/[$\bar{1}$ 11] (b) [1$\bar{1}$ $\bar{1}$]/[100]. The labelling of blocking dips refers to Figure 4.2. Note the poor match of the 57˚ (ε) blocking feature in the [$\bar{1}$ 00]/[$\bar{1}$ 11] geometry.

	Si_1–Tm (Å)	Si_2–Tm (Å)	Si_1–Si_2 (Å)
Vertical Distance	2.67 ± 0.02	1.77 ± 0.03	0.90 ± 0.03
Bond Length	N/A	2.84 ± 0.02	2.39 ± 0.02

Table 4.1: Structural parameters for the initial best model for the Tm silicide under discussion. The Si_1–Tm bond length is thought to be underestimated while the Si_1–Si_2 bond length is overestimated.

4.3.3   Re-examination of Best Fit Model

An examination of Figure 4.7 (a) shows that the blocking feature at around 57° is not particularly well fitted. Visual inspection of the comparison of experimental data and the structural models showed that some, at least quantitatively, fitted this dip more accurately whilst maintaining a comparable match to the rest of the data. As Figure 4.2 shows, the 57° blocking dip (labelled ε) is due purely to blocking of scattered ions by Si_2 atoms. Its position therefore directly relates to the atomic position of Si_2. Any failing of the fitting process which results in a solution being selected which is apparently not the best fit, as observed here, is therefore cause for concern.

Further investigation revealed that the depth of the lower blocking dip, at ~45° (γ in Figure 4.2), was having an unduly large influence on the R-factor, causing a failure to correctly fit the higher angle dip. Further discussion and justification for this conclusion may be found in the next chapter.

In light of the above discovery, the R-factor for the [$\bar{1}$ 00]/[$\bar{1}$ 11] geometry was recalculated, excluding the lower γ dip from the calculation (essentially the data for this geometry was cut off below about 47°. However, the main structural information is contained within the angular position of the dip. The γ dip is due to both Si_1 and Si_2. These atoms cause the other two dips in this geometry, so the positional information is contained within the remaining portion of data. This procedure was therefore felt to be justified in an effort to improve the high angle dip fit and therefore the accuracy of the Si_2 position). This led to a new best fit structural model, shown in Figure 4.8. It may be noted that the ~57° dip is now
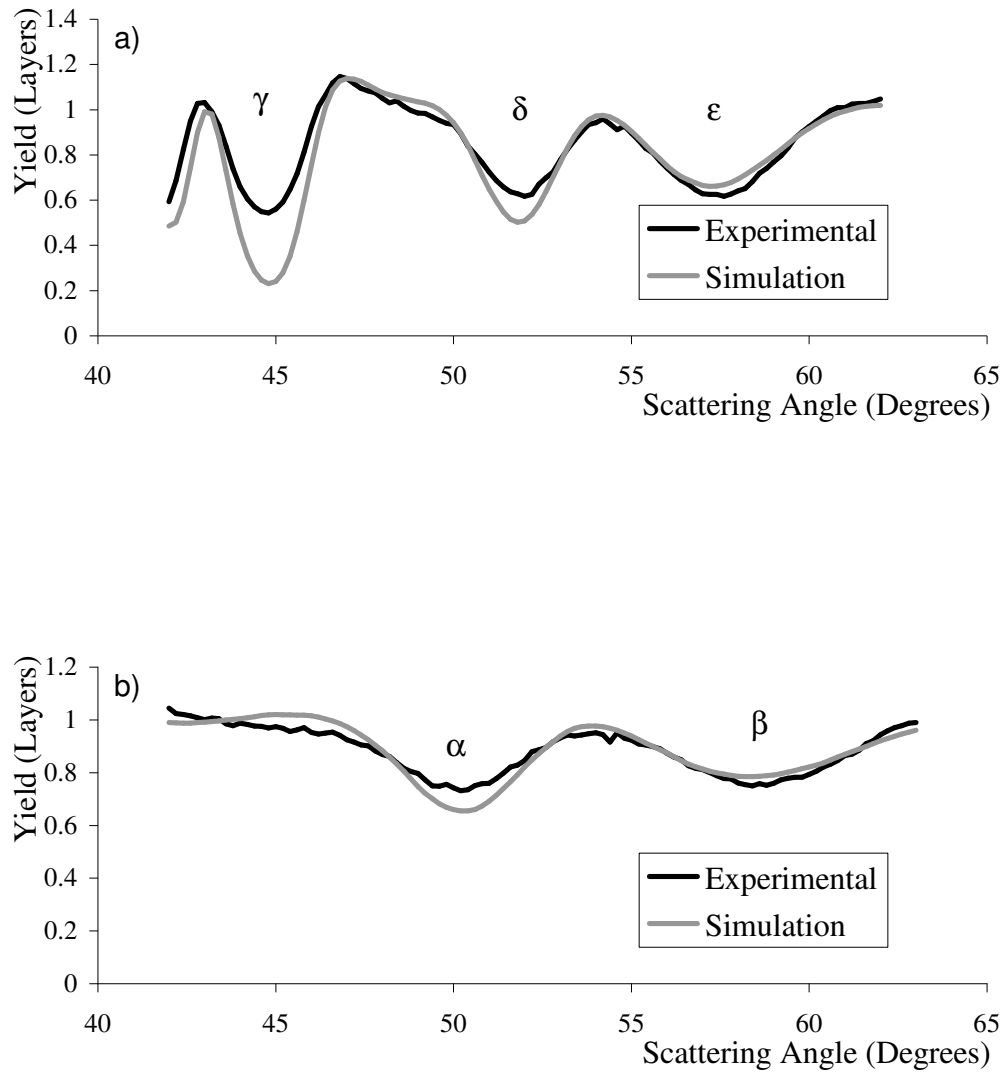
Figure 4.8: Comparison between experimental data and the simulated scattering curve for the final model for two-dimensional Tm silicide (again corrected for Rutherford scattering cross-section). The experimental yield is freely scaled to the simulation. (a) [$\bar{1}$ 00]/[$\bar{1}$ 11] (b) [1$\bar{1}$ $\bar{1}$]/[100]. The ~57˚ (ε) dip position is now visually a better fit.

	Si_1–Tm (Å)	Si_2–Tm (Å)	Si_1–Si_2 (Å)
Vertical Distance	2.66 ± 0.02	1.80 ± 0.02	0.86 ± 0.03
Bond Length	N/A	2.86 ± 0.02	2.38 ± 0.02

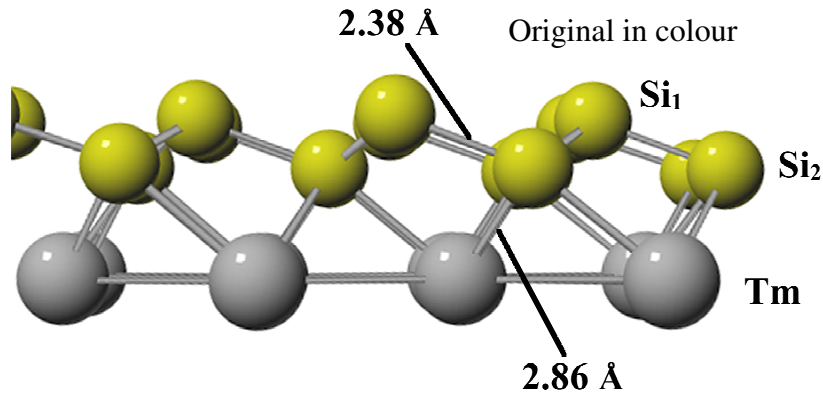*Table 4.2: Structural parameters for the final model for 2D Tm silicide.*

Figure 4.9: Ball and stick representation of the Tm 2D silicide surface, showing the bond lengths of Table 4.2.

visually much better fitted whilst other features seem to be reproduced as comparatively well as before. The structural parameters for this final model are given in Table 4.2 and shown in Figure 4.9.

The re-examination of the model fitting process has resulted in an upward movement of Si_2 compared with the initial result. It should also be noted that the two structures derived are within experimental error of each other. The structural parameters determined are comparable to those known for other two-dimensional rare-earth silicides [5, 8-13]. The Si–Si bond of the top bilayer represents a slight expansion compared with the bulk Si value of 2.35 Å whereas the Si–Tm bond length represents a significant contraction from the bulk value of 2.98 Å. Further discussion of the relationship between these structural parameters and those of other 2D silicides may be found in the next chapter.

The quantitative fit of the simulated scattering curve to the experimental data has been improved by the procedure described above. However, a close examination of the multiple simulations reveals it is still possible to achieve a slightly better

qualitative fit. By closely comparing the angular position of the minima of the major blocking dips in the experimental data and simulations, a further structural model was arrived at (in this procedure it was noted that from geometrical considerations the δ and ε dips are essentially independent of one another, as are the α and β dips, so each could be fitted separately. The change in structural model actually has very little affect on the angular position of the γ dip, which was therefore to some extent neglected) . The data–simulation comparison for this model is shown in Figure 4.10. The structural parameters are summarised in Table 4.3. It is difficult to estimate an error from such a subjective "by eye" fitting procedure. Those quoted are based on a consideration of the step size in the change of each parameter within the simulations and a subjective judgement as to when the fit becomes poor. Although the position of the Si_2 atoms differs slightly between the best by eye fit and the refined structural solution, the bond lengths are identical to within the precision possible with this technique. Further discussion of "by eye" fitting of 2D silicide models for other rare earth metals may be found in the next chapter.

4.4   Conclusion

It has been seen that depositing one monolayer of Tm onto the clean Si (111) 7×7 reconstruction and annealing to around 500 ˚C produces a reconstruction of the surface. This reconstruction results in a 1×1 LEED pattern. Medium energy ion scattering data have been taken from the surface and a structural analysis performed. The structure is seen to be extremely similar to that of other "two-dimensional " rare earth silicides, as was expected. The structural analysis has shown some possible failings in the reliance upon the χ^2 R-factor for guidance in comparing experimental data to simulations of multiple trial models. These problems are discussed more fully in the next chapter. Despite this, Monte Carlo simulations of ion scattering from the final model show good agreement with the experimental data for both scattering geometries used. A structural model has been proposed based upon this.
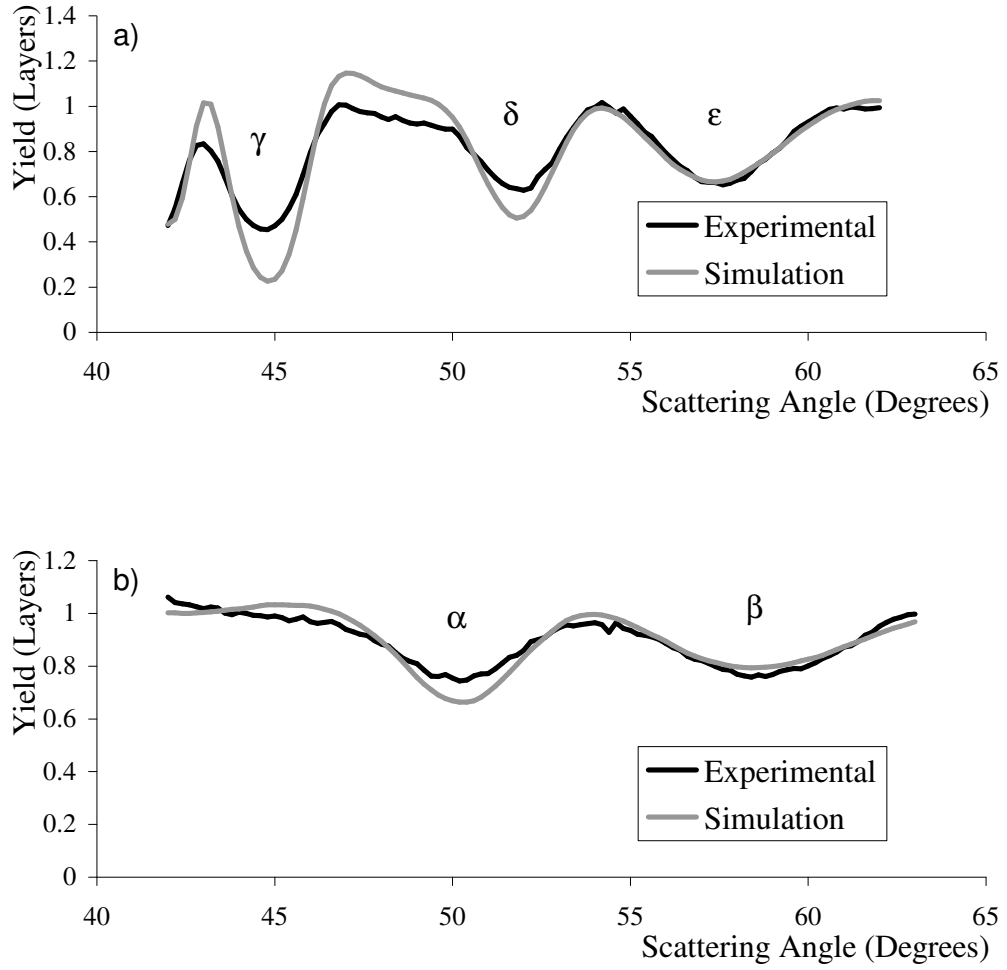
Figure 4.10: Comparison between experimental data and simulation for the "by eye" fit, corrected for Rutherford scattering cross-section. (a) [$\bar{1}$00]/[$\bar{1}$11] (b) [1$\bar{1}$ $\bar{1}$]/[100]. The ~57° (ε) dip position has been further improved.

	Si$_1$–Tm (Å)	Si$_2$–Tm (Å)	Si$_1$–Si$_2$ (Å)
Vertical Distance	2.66 ± 0.03	1.81 ± 0.04	0.85 ± 0.04
Bond Length	N/A	2.86 ± 0.02	2.38 ± 0.02

Table 4.3: Structural parameters determined from a "by eye" fit.

References

1.   J. A. Knapp and S. T. Picraux, *Appl. Phys. Lett.* **48** 466 (1986)

2.   A. Travlos, N. Salamouras and N. Boukos, *J. Appl. Phys.* **81** 1217 (1997)

3.   C. Wigren, J. N. Andersen, R. Nyholm and U. O. Karlsson, *J. Vac. Sci. Technol. A* **11** 2665 (1993)

4.   D. P. Spence and S. P. Tear, *Personal Communication* (2001)

5.   D. J. Spence, S. P. Tear, T. C. Q. Noakes and P. Bailey, *Phys. Rev. B* **61** 5707 (2000)

6.   VEGAS, *FOM Institute*

7.   D. P. Woodruff and T. A. Delchar, *Modern Techniques of Surface Science*, Cambridge University Press (1986)

8.   M. H. Tuilier, P. Wetzel, C. Pirri, D. Bolmont and G. Gewinner, *Phys. Rev. B* **50** 2333 (1994)

9.   C. Bonet, D. J. Spence and S. P. Tear, *Surf. Sci.* **504** 183 (2002)

10.   C. Rogero, C. Polop, L. Magaud, J. L. Sacedón, P. L. de Andrés and J. A. Martín-Gago, *Phys. Rev. B* **66** 235421 (2002)

11.   D. J. Spence, T. C. Q. Noakes, P. Bailey and S. P. Tear, *Surf. Sci.* **512** 61 (2002)

12.   M. Lohmeier, W. J. Huisman, G. ter Horst, P. M. Zagwijn, E. Vlieg, C. L. Nicklin and T. S. Turner, *Phys. Rev. B* **54** 2004 (1996)

13.   H. Kitayama, S. P. Tear, D. J. Spence and T. Urano, *Surf. Sci.* **482-485** 1481 (2001)